The QE numerical simulation of PEA semiconductor photocathode

LI Xu-Dong(李旭东)[1,2;1)] GU Qiang(顾强)[1]
ZHANG Meng(张猛)[1] ZHAO Ming-Hua(赵明华)[1;2)]

[1] Shanghai Institute of Applied Physics, Chinese Academy of Sciences, Shanghai 201800, China
[2] Graduate University of the Chinese Academy of Sciences, Beijing 100049, China

Abstract: Several kinds of models have already been proposed to explain the photoemission process. The exact photoemission theory of the semiconductor photocathode was not well established after decades of research. In this paper an integral equation of quantum efficiency (QE) is constructed to describe the photoemission of positive electron affinity (PEA) of the semiconductor photocathode based on the three-step photoemission model. Various factors (e.g., forbidden band gap, electron affinity, photon energy, incident angle, degree of polarization, refractive index, extinction coefficient, initial and final electron energy, relaxation time, external electric field and so on) have an impact on the QE of the PEA semiconductor photocathode, which are entirely expressed in the QE equation. In addition, a simulation code is also programmed to calculate the QE of the K_2CsSb photocathode theoretically at 532 nm wavelength. By and large, the result is in line with the expected experimental value. The reasons leading to the distinction between the experimental and theoretical QE are discussed.

Key words: photocathode, quantum efficiency, K_2CsSb, simulation

PACS: 79.60.-i, 71.20.Nr, 72.20.Dp **DOI:** 10.1088/1674-1137/36/6/009

1 Introduction

Generally speaking, the relevant property that characterize photocathodes are: QE, operational lifetime, response time, emittance, emission uniformity, dark current, damage threshold, etc. Metallic and semiconductor photocathodes [1] are routinely used in high brightness, low transverse emittance and high average current photoinjector. Metallic photocathodes have a prompt response time, they are insensitive to contamination and easy to manufacture and operate in high electric field. They have small electron beam emittance and dark current, but poor quantum efficiency (QE) with ultraviolet radiation. In contrast, semiconductor photocathodes have different characteristics of the highest QE at longer wavelengths, however, they are sensitive to contamination and have a slow response time.

The bialkali photocathodes can commonly be used in a photocathode electron gun since they have higher QE, lower emittance and dark currents than other photocathodes. K_2CsSb [2] is the most typical bialkali photocathode, which is operated under the visible light irradiation, that means more available power and stable drive laser system.

The researchers not only make the utmost effort to discover and prepare the superior photocathode, but also devote themselves to developing a photoemission theory for various photocathodes. So far, the most successful photoemission model is the three-step photoemission model. Although the model does not include any of the specific surface effects and assumes that the photoelectrons which diffuse to the photocathode-vacuum surface and escape from the surface are processed independently, it has been successfully used to interpret the photoelectron emitting process of elemental metal, metallic compound, alkali antimonide, alkali telluride, alkali halide, and the III-V photocathode [3–6]. In the following section, an approximate QE equation of reflection mode positive

Received 30 August 2011
1) E-mail: lixudong@sinap.ac.cn
2) E-mail: zhaominghua@sinap.ac.cn

electron affinity (PEA) semiconductor photocathode based on previous theoretical and experimental results is obtained and validated.

2 Derivation of the QE equation of PEA semiconductor photocathode

QE is the most basic and important characteristic of the photocathode, which is the number of photoelectrons emitted from the photocathode divided by the number of incident photons. The semiconductor energy band diagram is shown in Fig. 1. h is the Plank constant, ν is the light frequency, $E_{\rm VBM}$ is the valence band maximum, $E_{\rm CBM}$ is the conduction band minimum, $E_{\rm VAC}$ is the vacuum level, $E_{\rm F}$ is the Fermi level, and $E'_{\rm VAC}$ is the vacuum level after the schottky effect reduction. $\Delta E_{\rm a}$ is the external electric field induced electron affinity decrease, $E_{\rm g}$ is the forbidden band gap which cannot be occupied by electrons, and $E_{\rm a}$ is the electron affinity, which is the interval between the conduction band minimum and the vacuum level.

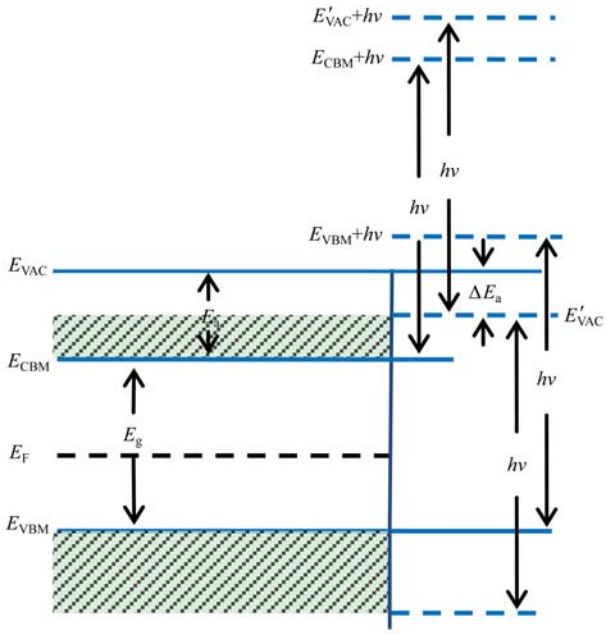

Fig. 1. The simplified energy band diagram of PEA semiconductor photocathode.

It is well known that the semiconductor photocathode is illuminated with light in the external accelerating electric field when photon energy is greater than the sum of the forbidden band gap and the electron affinity, the bound electrons in the valence band and conduction band will absorb photon energy, and then emit from the photocathode interior to vacuum as photoelectrons. Spicer's three-step photoemission model [7] is used to explain the process. Each step of the model has an associated probability. QE is just the product of these probabilities in the photoemission process, which is simply given by

$$QE=\int_{E_{\rm bottom}}^{E_{\rm top}} P\left(E,h\nu,T\right)F_{\lambda}\left(s,E,\nu,\theta\right)D\left(E\right){\rm d}E, \tag{1}$$

where E is the electron energy; $E_{\rm bottom}$, $E_{\rm top}$ are the bottom and top electron energy of the valence and conduction band in semiconductor，respectively; $P(E,h\nu,T)$ is the probability of the electron to change from the initial state of energy E to the final state of energy $E+h\nu$; T is the photocathode temperature; $F_{\lambda}(s,E,\nu,\theta)$ is the probability that the photoelectron arrives at the photocathode surface after undergoing several scatterings; s is the depth; θ is the angle of the photoelectron velocity relative to the surface normal; $D(E)$ is the probability for photoelectron to enter vacuum.

Step 1: Absorb photons and excite electrons

The number of photoelectrons is determined by the number of photons that can be absorbed and the number of electrons that can be excited in the first step of the three-step photoemission model. We hypothesize the photoelectrons are from the valence band and conduction band of semiconductor photocathode respectively, the probability $P(E,h\nu,T)$ is solely the function of $\rho_{\rm EDOS}(E)$, $f_{\rm FD}(E,T)$, $\rho_{\rm EDOS}(E+h\nu)$, and $f_{\rm FD}(E+h\nu,T)$, which can be written as

$$P\left(E,h\nu,T\right)=\left(1-R\right)\times\frac{\rho_{\rm EDOS}(E+h\nu)\left(1-f_{\rm FD}\left(E+h\nu,T\right)\right)\rho_{\rm EDOS}(E)f_{\rm FD}\left(E,T\right)}{\int_{E_{\rm VBM}}^{E_{\rm VBM}+h\nu}{\rm d}E'\,\rho_{\rm EDOS}(E'+h\nu)\left(1-f_{\rm FD}\left(E'+h\nu,T\right)\right)\rho_{\rm EDOS}(E')f_{\rm FD}\left(E',T\right)}$$

$$\frac{+\rho_{\rm EDOS}(E+h\nu)\left(1-f_{\rm FD}\left(E+h\nu,T\right)\right)\rho_{\rm EDOS}(E)f_{\rm FD}\left(E,T\right)}{+\int_{E_{\rm CBM}}^{E_{\rm CBM}+h\nu}{\rm d}E'\,\rho_{\rm EDOS}(E'+h\nu)\left(1-f_{\rm FD}\left(E'+h\nu,T\right)\right)\rho_{\rm EDOS}(E')f_{\rm FD}\left(E',T\right)}, \tag{2}$$

the denominator represents a normalization based on the assumption of the 100% absorption of photons.

In general, the reflectivity R is a function of incident light wavelength, incident angle ϕ, polarization state of incident light, refractive index n, extinction coefficient k and photocathode thickness. n and k are also relative to photon energy, with n and k in hand, R as a function of polarization state is obtained from Ref. [8]

$$R=\frac{1}{2}\left[R_{\mathrm{p}}(1+p)+R_{\mathrm{s}}(1-p)\right], \tag{3}$$

here R_{s} is the component of reflection perpendicular to the plane of incidence, and R_{p} is the parallel component. The degree of polarization p for the incident light is given by $p=(I_{\mathrm{p}}-I_{\mathrm{s}})/(I_{\mathrm{p}}+I_{\mathrm{s}})$, I_{p} and I_{s} are the parallel and perpendicular component of light intensity respectively.

$\lambda_{\mathrm{opt}}(\nu)$ is the penetration depth (i.e., skin depth), which is also as a function of n and k, $\lambda_{\mathrm{opt}}(\nu)$ can be usually simplified as the inverse of the absorption coefficient α,

$$\lambda_{\mathrm{opt}}(\nu)=1/\alpha=\lambda/4\pi nk. \tag{4}$$

As everyone knows, the electron distribution of semiconductor photocathode material is the Fermi-Dirac distribution

$$f_{\mathrm{FD}}(E,T)=\frac{1}{1+\exp\left(\dfrac{E-E_{\mathrm{F}}}{k_{\mathrm{B}}T}\right)}, \tag{5}$$

here k_{B} is the Boltzmann constant; and E_{F} is the Fermi level, the approximate formula is

$$E_{\mathrm{F}}=\frac{E_{\mathrm{VBM}}+E_{\mathrm{CBM}}}{2}. \tag{6}$$

Step 2: Migrate to surface

The second step of the three-step photoemission model is that a photoelectron moves to the photocathode surface. The assumption of the exponential model about the photoelectron transport is the average effect of plenty of nearly elastic and inelastic collisions when the photocathode thickness is much greater than the photoelectron scattering length. Therefore, the fraction of photoelectrons per unit distance at a depth s from the surface, which avoids scattering is given by

$$F_{\lambda}(s,E,\nu,\theta)=\frac{\displaystyle\int_0^{\infty}\exp\left(-\frac{s}{\lambda_{\mathrm{opt}}(\nu)}-\frac{s}{l(E)\cos\theta}\right)\mathrm{d}s}{\displaystyle\int_0^{\infty}\exp\left(-\frac{s}{\lambda_{\mathrm{opt}}(\nu)}\right)\mathrm{d}s}=\frac{\cos\theta}{\cos\theta+\sqrt{\dfrac{m}{2E}}\dfrac{\lambda_{\mathrm{opt}}(\nu)}{\tau(E)}}, \tag{7}$$

where m is the effective electron mass, which is related to the forbidden band gap via $m/m_0=E_{\mathrm{g}}/R_{\infty}$, R_{∞} is the Rydberg constant, m_0 is the free electron mass. $\tau(E)$ is the relaxation time, $l(E)=v(E)\tau(E)=\sqrt{2E/m}\,\tau(E)$, $l(E)$ is the scattering length, and $v(E)$ is the electron velocity. The photoelectrons may lose energy and change the direction of movement by colliding with other electrons (electron-electron scattering), lattices (electron-phonon scattering) and impurities (electron-impurity scattering) in the course of photoelectrons diffusing from the photocathode interior to the photocathode-vacuum interface. The general diffusion model has been presented by Kane, which includes the scattering length from electron-electron, electron-phonon and other scattering interactions. According to the above discussion, $\tau(E)$ follows the Matthiessen's Rule with the relationship of various scatterings [9]

$$\tau_{\mathrm{total}}^{-1}=\sum_j\tau_j^{-1}. \tag{8}$$

Due to the small number of free electrons in the conduction band in the semiconductor, the electron-electron scattering is negligible when the photoelectron is moving towards the surface-vacuum interface. The electron-impurity scattering effect on photoelectron transmission can be minimized by reducing the impurity concentration, optimizing the crystal size and orientation. The primary scattering is dominated by electron-phonon scattering (the energy loss is rather small through electron-phonon scattering, which will mainly change the moving direction of photoelectron). It is obvious that the electron-phonon scattering contains polar optical phonon scattering and acoustic phonon scattering. The previous researchers [9] have found that the contribution of acoustic phonon scattering for the relaxation time is small compared with the polar optical phonon scattering, therefore the impact of polar optical phonon scattering on relaxation time is only considered. The equation of relaxation time originating from the optical phonon scattering is analogous to the Cs_3Sb photocathode (The format is shown as in Ref. [9]). The differences are the high frequency dielectric constant ε_{∞} given approximately by the Drude theory expression, $\varepsilon_{\infty}=n^2$ and the static dielectric constant $\varepsilon_0\approx n^2+k^2$, so

$$\Delta\varepsilon=1/n^2-1/(n^2+k^2). \tag{9}$$

Step 3: Escape from the surface

The third step of the three-step photoemission model is the photoelectrons with an energy component directed into a surface barrier greater than the surface barrier height which can successfully overcome the surface barrier after undergoing all kinds of scattering events, and then enter vacuum. The perpendicular component of the photoelectron momentum must satisfy [3]

$$\frac{\hbar^2 k_\perp^2}{2m} > E_{\rm VBM} + E_{\rm g} + E_{\rm a} - \Delta E_{\rm a}, \tag{10}$$

where $\Delta E_{\rm a}$ is the electric field induced electron affinity decrease of the semiconductor photocathode by the Schottky effect. In view of the property of the semiconductor photocathode and the equation of metallic Schottky effect, the reduction of electron affinity is described by

$$\Delta E_{\rm a} = \sqrt{\frac{\varepsilon - 1}{\varepsilon + 1}\beta q^3 E_{\rm D}}, \tag{11}$$

here ε is the dielectric constant of semiconductor photocathode, $\varepsilon \approx \varepsilon_0$ for low frequency electric field; e is the electron charge; $E_{\rm D}$ is the external electric field strength, $E_{\rm D} = V/d$, V is the applied voltage and d is the distance between the cathode and anode; β is the dimensionless effective field enhancement factor of photoemission.

In order to describe the photoelectron which escapes from interior to vacuum, the maximum emission angle $\theta_{\max}(E)$ of the photoelectron with enough energy to enter vacuum as follows

$$\theta_{\max}(E) = \cos^{-1}\left(\sqrt{\frac{E_{\rm VBM} + E_{\rm g} + E_{\rm a} - \Delta E_{\rm a}}{E + h\nu}}\right). \tag{12}$$

Eq. (12) is suitable for explaining the photoemission of the valence band and conduction band. The photoelectron may move to any direction of cathode internal when $\theta_{\max}(E)$=0 to π. For $\theta_{\max}(E)$ >0, the probability of the photoelectron to enter vacuum is given by

$$D(E) = \frac{\frac{1}{4\pi}\int_0^{\theta_{\max}(E)} \sin\theta {\rm d}\theta \int_0^{2\pi} {\rm d}\varphi}{\frac{1}{4\pi}\int_0^{\pi} \sin\theta {\rm d}\theta \int_0^{2\pi} {\rm d}\varphi} = \frac{1}{2}\int_0^{\theta_{\max}(E)} \sin\theta {\rm d}\theta. \tag{13}$$

From Eq. (1), Eq. (2), Eq.(7) and Eq. (13), the QE equation is

$$\begin{aligned}{\rm QE} = (1-R)\times & \frac{\int_{E_{\rm VBM}+E_{\rm g}+E_{\rm a}-\Delta E_{\rm a}-h\nu}^{E_{\rm VBM}} {\rm d}E A(E,h\nu,T) \int_0^{\theta_{\max}} \sin\theta {\rm d}\theta \int_0^{\infty} \exp\left(-\frac{s}{\lambda_{\rm opt}(\nu)} - \frac{s}{l(E)\cos\theta}\right) {\rm d}s \int_0^{2\pi} {\rm d}\varphi}{\int_{E_{\rm VBM}+E_{\rm g}+E_{\rm a}-\Delta E_{\rm a}-h\nu}^{E_{\rm VBM}} {\rm d}E A(E,h\nu,T) \int_0^{\pi} \sin\theta {\rm d}\theta \int_0^{\infty} \exp\left(-\frac{s}{\lambda_{\rm opt}(\nu)}\right) {\rm d}s \int_0^{2\pi} {\rm d}\varphi} \\ & + \frac{\int_{E_{\rm VBM}+E_{\rm g}}^{E_{\rm VBM}+E_{\rm g}+E_{\rm a}-\Delta E_{\rm a}} {\rm d}E A(E,h\nu,T) \int_0^{\theta_{\max}} \sin\theta {\rm d}\theta \int_0^{\infty} \exp\left(-\frac{s}{\lambda_{\rm opt}(\nu)} - \frac{s}{l(E)\cos\theta}\right) {\rm d}s \int_0^{2\pi} {\rm d}\varphi}{+\int_{E_{\rm VBM}+E_{\rm g}}^{E_{\rm VBM}+E_{\rm g}+E_{\rm a}-\Delta E_{\rm a}} {\rm d}E A(E,h\nu,T) \int_0^{\pi} \sin\theta {\rm d}\theta \int_0^{\infty} \exp\left(-\frac{s}{\lambda_{\rm opt}(\nu)}\right) {\rm d}s \int_0^{2\pi} {\rm d}\varphi},\end{aligned} \tag{14}$$

here

$$A(E,h\nu,T) = \rho_{\rm EDOS}(E+h\nu)\left(1 - f_{\rm FD}(E+h\nu,T)\right)\rho_{\rm EDOS}(E) f_{\rm FD}(E,T). \tag{15}$$

When the photocathode temperature is low, $k_{\rm B}T \ll E_{\rm F}$, the Fermi-Dirac distribution is well represented by the Heaviside-step function

$$\int_{E_{\rm bottom}}^{E_{\rm top}} {\rm d}E \left(1 - f_{\rm FD}(E+h\nu,T)\right) f_{\rm FD}(E,T) = \int_{E_{\rm bottom}}^{E_{\rm top}} {\rm d}E. \tag{16}$$

Substitute Eq. (16) into Eq. (14) and calculate; the QE equation is simplified as

$${\rm QE} = (1-R)\times \frac{\int_{E_{\rm VBM}+E_{\rm g}+E_{\rm a}-\Delta E_{\rm a}-h\nu}^{E_{\rm VBM}} B(\nu,\theta,E)C(E){\rm d}E + \int_{E_{\rm VBM}+E_{\rm g}}^{E_{\rm VBM}+E_{\rm g}+E_{\rm a}-\Delta E_{\rm a}} B(\nu,\theta,E)C(E){\rm d}E}{2\int_{E_{\rm VBM}+E_{\rm g}-h\nu}^{E_{\rm VBM}} C(E){\rm d}E + 2\int_{E_{\rm VBM}+E_{\rm g}}^{E_{\rm VBM}+E_{\rm g}+E_{\rm a}-\Delta E_{\rm a}} C(E){\rm d}E}, \tag{17}$$

here

$$B(\nu,\theta,E) = \int_{\cos\theta_{\max}(E)}^{1} \frac{\cos\theta}{\cos\theta+\sqrt{\frac{m}{2E}}\frac{\lambda_{\rm opt}(\nu)}{\tau(E)}}\mathrm{d}(\cos\theta) = 1-\sqrt{\frac{m}{2E}}\frac{\lambda_{\rm opt}(\nu)}{\tau(E)}\times\ln\left[1+\sqrt{\frac{m}{2E}}\frac{\lambda_{\rm opt}(\nu)}{\tau(E)}\right]$$

$$-\cos\theta_{\max}+\sqrt{\frac{m}{2E}}\frac{\lambda_{\rm opt}(\nu)}{\tau(E)}\ln\left[\cos\theta_{\max}+\sqrt{\frac{m}{2E}}\frac{\lambda_{\rm opt}(\nu)}{\tau(E)}\right], \quad (18)$$

$$C(E) = E^{1/2}(E+h\nu)^{1/2}.$$

3 The verification of the QE equation based on the K_2CsSb photocathode

The experimental results of n and k from D. Motta and S. Hallensleben [10, 11] are shown in Fig. 2. Table 1 shows n=3.3 and k=0.8, when thin K_2CsSb photocathode is irradiated with 532 nm light.

The sound velocity v_s is inferred from the elastic constant c_{11} and the mass density ρ by the relationship $v_s = \sqrt{c_{11}}/\rho$ [9]. ρ is the ratio of the mass of atoms in a unit cell with the unit cell volume L^3 of K_2CsSb, L is lattice constant. The K_2CsSb crystal structure is DO_3 cubic (O_h^5 space group [12]), the unit cell contains four K_2CsSb units, that is

$$\rho = \frac{4(2m_{\rm K}+m_{\rm Cs}+m_{\rm Sb})}{L^3} = 3.4643\ \mathrm{g/cm^3}, \quad (19)$$

$m_{\rm Cs}$=2.21×10^{-22} g ($m_{\rm Cs}$ is the mass of each cesium atom), $m_{\rm Sb}$=2.02×10^{-22} g, $m_{\rm K}$=6.49×10^{-23} g and c_{11} is a "generic" semiconductor value of 12×10^{11} N/m^2. The phonon energy $\hbar\omega_q$ is crudely related to the sound velocity in the relation suggested by Ridley of $\hbar\omega_q \approx 4\pi\hbar v_s/L \approx 0.5654$ eV, the value is slightly larger than Cs_3Sb. $\omega_q \approx 4\pi v_s/L$=8.5899×10^{13} Hz, ω_q is phonon frequency. These parameters in simulation are given in Table 1.

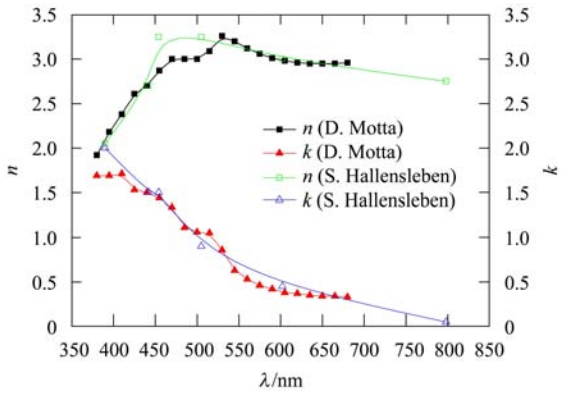

Fig. 2. (color online) The refractive index and extinction coefficient versus the wavelength of K_2CsSb photocathode.

Table 1. Parameters used in simulation for K_2CsSb photocathode.

symbol	value
E_g/eV	1.2
E_a/eV	0.7
$E_{\rm VBM}$/eV	1.27
λ/nm	532
ϕ	π/12
n	3.3
k	0.8
p	−99/101
T/K	300
E_D/(V/m)	2×10^4
β	1
L/Å	8.61
v_s/(m/s)	5885.5
h/(J·s)	4.136×10^{-15}
R_∞/eV	13.606
e/C	1.60×10^{-19}
k_B/(eV/K)	8.62×10^{-5}

4 Result and discussion

QE is 4.69% when 532 nm light is used to irradiate the K_2CsSb photocathode. The theoretical result is in agreement with the experimental value of some institutes. For example, photocathode with QE of 4.2% at 532 nm wavelength light was irradiated at Cornell University [13, 14]. The maximum QE measured is typically 6% at 532 nm at LBNL [15], when the K_2CsSb photocathode is evaporated on Mo or stainless steel substrate. Nevertheless, there is plenty of disagreement between theoretical and experimental QE. The reasons will be listed as follows:

Firstly, as a matter of fact, the drive light is not absolutely monochromatic. Secondly, the composition of the K-Cs-Sb photocathode is not really K_2CsSb, because the stoichiometry of alkali antimonide varies with the photocathode depth. The QE

of the alkali antimonide compound has been measured in experiments. Thirdly, the absorption coefficient of the K_2CsSb photocathode has been calculated by L. Kalarasse [16], which is different from the equation value via $\alpha = 4\pi nk/\lambda$. Actually, the absorption coefficient can be obtained by not calculating from n, k and λ, which is only measured accurately by experimental methods. Fourthly, other scattering effects on relaxation time have been omitted with only the polar photon scattering considered. Fifthly, the Fermi-Dirac distribution is not precisely replaced by the Heaviside-step function at the non-absolute zero. Sixthly, the uncertainly of the Fermi level of K_2CsSb from different impurity concentration gives rise to the deviation. Finally, the measured forbidden band gap and electron affinity of the K_2CsSb photocathode by different institutes [17] are shown in Table 2.

Table 2. The forbidden band gap and electron affinity of the K_2CsSb photocathode.

	E_g/eV	E_a/eV
NRL	1.1	0.65
BARC	1.2	0.7
BNL	1.0	1.1

The dependence of QE on the angle of incident light, the polarization state of incident light, the applied bias voltage and the photocathode temperature with certain photon energy has also been simulated as shown in Fig. 3. It is found that the QE of the K_2CsSb photocathode changes with the incident angle of light quickly. The influence of photocathode temperature, degree of polarization of incident light and electric field on QE can be neglected under certain conditions.

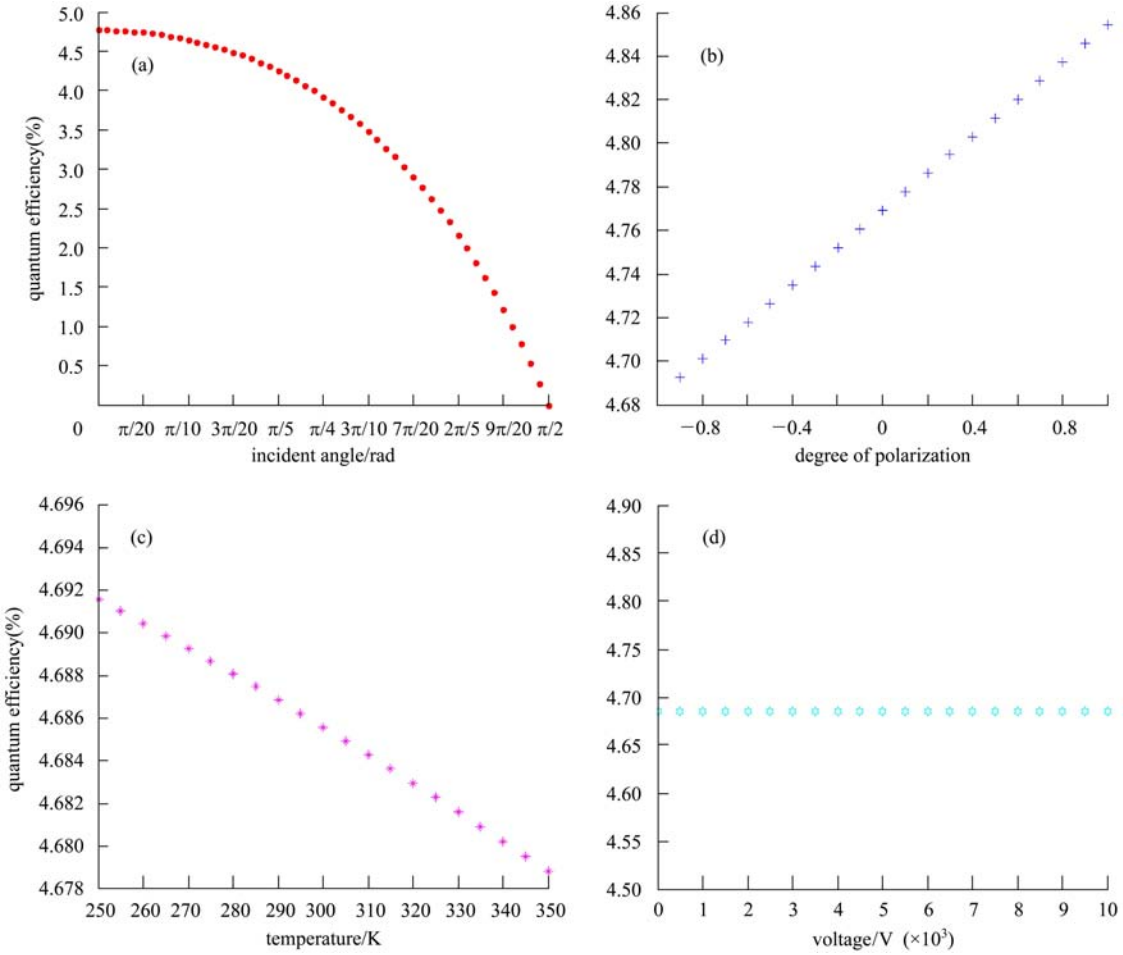

Fig. 3. QE as a function of incident angle of light (a), degree of polarization of light (b), photocathode temperature (c) and the external accelerating electric field (d) at 532 nm wavelength of the K_2CsSb photocathode respectively.

5 Conclusion

In summary, an approximate photoemission model is developed and verified to be capable of explaining photoemission process of the PEA semiconductor photocathode. The probabilities of photon absorption, photoelectron diffusion and photoelectron escape are all embodied in the QE equation. It is found that QE is 4.69% and identifies the different effects of incident angle, polarization state, photocathode temperature and external electric field on QE in simulation. This research could be useful not only for the study of pre-existing photocathodes, but also for the discovery of the new high efficient photocathode.

The authors would like to thank Erdong Wang of BNL for his beneficial discussions about the theory of photoemission.

References

1 Dowell D H et al. Nucl. Instrum. Methods A, 2010, **622**(3): 685–697
2 Burrill A et al. Multi-alkali photocathode development at Brookhaven National Lab for application in superconducting photoinjectors. In: Proceedings of PAC. 2005, Tennessee, USA, 2005. 2672–2674
3 Dowell D H et al. Phys. Rev. Spec. Top-Ac, 2006, **9**(6): 063502
4 Dowell D H, Schmerge J F. Phys. Rev. Spec. Top-Ac, 2009, **12**(7): 074201
5 Smedley J et al. Phys. Rev. Spec. Top-Ac, 2008, **11**(1): 013502
6 Smedley J et al. J. Appl. Phys., 2005, **98**(4): 043111
7 Spicer W E, Herrera-Gomez A. Modern theory and applications of photocathodes. In: Proceeding of SPIE 2022. San Diego, USA, 1993. 18–33
8 Jensen K L et al. J. Appl. Phys., 2006, **99**(12): 124905
9 Jensen K L et al. J. Appl. Phys., 2008, **104**(4): 044907
10 Hallensleben S et al. Opt. Commun, 2000, **180**(1–3): 89–102
11 Motta D, Schonert S. Nucl. Instrum. Methods A, 2005, **539**(1–2): 217–235
12 Kalarasse L et al. J. Phys. Chem. Solids, 2010, **71**(3): 314–322
13 Bazarov I et al. Appl. Phys. Lett., 2011, **98**(22): 224101
14 Cultrera. L et al. Growth And Characterization of Bialkali Photocathodes For Cornell ERL Injector. In: Proceedings of PAC2011. New York, USA. URL:www.c-ad.bnl.gov/pac2011/proceedings/papers/wep244.pdf
15 Vecchione T et al. Appl. Phys. Lett., 2011, **99**(3): 034103
16 Kalarasse L et al. J. Phys. Chem. Solids, 2010, **71**(12): 1732–1741
17 Ghosh C, Varma B P. J. Appl. Phys., 1978, **49**(8): 4549–4553